Exploiting the kinetic interplay between the GPIbα–VWF binding interfaces to regulate hemostasis and thrombosis

Jianchung Chen,[1] Hairu Zhou,[1] Alexander Diacovo,[1] X. Long Zheng,[3] Jonas Emsley,[4] and Thomas G. Diacovo[1,2]

[1]Department of Pediatrics, Columbia University Medical Center, New York, New York, 10032, USA. [2]Department of Pathology and Cell Biology, Columbia University Medical Center, New York, New York, 10032, USA. [3]Department of Pathology and Laboratory Medicine, The Children's Hospital of Philadelphia, Philadelphia, Pennsylvania, 19104 USA. [4]Centre for Biomolecular Sciences, School of Pharmacy, University of Nottingham, University Park, Nottingham, NG72RD, UK.

Correspondence

Thomas Diacovo, MD
Columbia University
1130 St. Nicholas Ave, Room 924
New York, NY 10032
Tel: 212-851-4683
E-mail: td2142@cumc.columbia.edu

Short title: Regulating adhesion between platelets and VWF

Text word count: 4,341
Text abstract count: 200
Number of figures: 6, and 2 supplemental figures
Number of tables: 1
Number of references: 43

Key points

- GPIbα–VWF-A1 bond lifetime governs platelet–VWF interactions and can be altered to correct defects in hemostasis or prevent thrombosis.

- Targeting a distinct binding interface between GPIbα and VWF-A1 offers a unique therapeutic approach to reducing platelet-driven thrombosis

Abstract

Platelet–VWF interactions are tightly controlled to prevent vascular occlusion due to premature aggregate formation. Although multiple mechanisms may regulate this process, it is unclear whether the inherent properties of the bond formed the platelet receptor GPIbα and the A1 domain of VWF can influence the site and extent to which platelets bind VWF. Here, we demonstrate that the kinetic interplay between two distinct regions of contact between this receptor–ligand pair not only permit maximal platelet accrual at sites of arterial injury, but can be manipulated to correct defective hemostasis or prevent thrombosis. This was accomplished by generating VWF-A1 knock-in mice with mutations that enhance (I1309V) or disrupt (R1326H) GPIbα binding and by targeting the complex with an allosteric inhibitor. Incorporation of R1326H mutation in the major site shortened bond lifetime, yielding defects in hemostasis and thrombosis comparable to VWF deficient animals. Similarly, pharmacologic disruption of the major interface prevented arterial thrombosis. However, combining the R1326H mutation with the I1309V mutation located near the minor site normalized bond kinetics and restored the hemostatic and thrombotic properties of VWF. Hence, an important biophysical-–biological relationship is revealed and the therapeutic benefits of modifying the GPIbα–VWF-A1 binding interfaces established.

Introduction

The ability of blood borne cells to perform their designated biological function(s) requires cell surface adhesion molecules to engage counter-receptors at the appropriate time and location. For example, platelets and von Willebrand factor (VWF) co-exist in circulating blood and must interact at sites of arterial injury in order to promote effective hemostasis. This process is triggered upon the binding of plasma VWF to exposed components of the injured vessel wall where it can then initiate the attachment of platelets under shear flow conditions.[1,2] VWF is a multimeric plasma glycoprotein composed of functionally distinct types of domains that are either duplicated or triplicated in the following order from the N-terminus: D'-D3-A1-A2-A3-D4-B1-B2-B3-C1-C2-CK.[3,4] It is the interaction between VWF-A1 domain and the platelet receptor glycoprotein Ib alpha (GPIbα) that initiates primary hemostasis by bringing platelets into close proximity with reactive substrates generated at the site of arterial damage.[5-8] The clinical significance of this interaction is underscored by the increased bleeding tendencies of individuals who either lack the plasma protein or possess mutations within the A1 domain of VWF. In the latter case, this includes mutations that limit binding (type 2M) or paradoxically enhance interactions (type 2B), both of which are associated with the hereditary bleeding disorder known as von Willebrand disease (VWD).[3,4]

Against this background, structure analyses of native and mutant complexes have provided insights into the nature of the interactions that support adhesion between this receptor–ligand pair and possible mechanisms by which mutations alter this process. The structure reveals a major and minor binding site for GPIbα on the surface of the A1 domain that is bridged by an area of solvated charge interaction.[9,10] Type 2M mutations,

located in or directly adjacent to the larger contact surface, may disrupt electrostatic interactions between this receptor–ligand pair or induce structural changes that reduce GPIbα binding. In contrast, type 2B mutations are clustered in close proximity to the minor site near the termini of the domain and may alter the conformation of a region known as the α1-β2 loop.[9-12] Consequently, this is thought to provide an essential energetic contribution that augments binding affinity[9] or reduce a steric clash that would impede adhesion.[13] Clinically, this enhanced binding is believed to result in bleeding by permitting VWF multimers with the greatest hemostatic potential to aggregate spontaneously with platelets in blood and ultimately be cleared from the circulation.[3,4] Although such studies provide insight into mechanism(s) by which mutations associated with VWD may alter binding between platelets and VWF, they cannot account for interactions involving sites outside of the A1 and GPIbα binding domains or external influences such as shear flow that play a role in regulating hemostasis and thrombosis.[14] Indeed, several mechanisms have been identified that may prevent VWF–platelet aggregate formation in the circulation. This includes shielding of VWF-A1 by the adjacent D'D3 domains,[15] the inhibitory effects of the β2-glycoprotein I,[16] and the ability of shear flow to activate the VWF-A1 so that it can then engage GPIbα.[17] Moreover, it has been demonstrated that forces generated by flowing blood can promote the unfolding and elongation of VWF so that it exposes multiple A1 domains.[18]

An additional mechanism that has not been fully explored is the contribution that the physicochemical properties of the bond formed between VWF-A1 and GPIbα play in regulating platelet–VWF interactions at sites of vascular injury. Indeed, detailed analyses of the kinetic and mechanical properties of this receptor–ligand pair have yielded insight

into the biophysical consequences of the predicted allosteric change associated with type 2B mutations.[19-22] That said, it remains unclear whether specific properties of the GPIbα–VWF-A1 bond predicted to regulate platelet–VWF interactions correspond with biological reality.[23-25]

In the current study, we address this shortcoming by performing a detailed kinetic analysis of WT and mutant murine GPIbα–VWF-A1 complexes and then validating these observations using transgenic mice harboring modified VWF-A1 domains. We also probe the binding interface using a novel allosteric inhibitor that prevents the formation of key interactions between this receptor–ligand pair. Our data reveal that the physicochemical properties of the distinct regions of contact between this receptor–ligand pair contribute to a composite biophysical signature required for effective hemostasis and arterial thrombus formation.

Methods

Modeling of murine GPIbα–VWF-A1 complexes

Crystal structures of the human GPIbα–VWF-A1 complex have been described for WT and for the complex formed between the GOF mutations R1306Q and I1309V in VWF-A1 and the platelet type GOF mutation M239V in GPIbα.[9,10,13,26] The human platelet receptor was used as a template for mouse GPIbα. Consensus rotamers with minimal steric clashes were chosen, followed by adjustments to create reasonable van der Waals interactions and H-bonding using COOT (http://www.biop.ox.ac.uk/coot/).

A consensus model of the human receptor–ligand pair was used to build its murine counterpart. This included the double mutant VWF-A1 (I1309V, R1326H) complex that was based on the human VWF-A1 (R1306Q) mutant complex using the program SWISSMODEL (http://swissmodel.expasy.org/).[10] Figures were created using PYMOL.

Mice

The generation of the VWF^{R1326H} mutant mouse has been previously described.[27] A similar targeting strategy was used to introduce the double mutation I1309V, R1326H into exon 28 of the murine VWF gene or to substitute in the human A1 domain. VWF deficient mice were purchased from The Jackson Laboratory. All animals were on a C57BL/6J background and kept in a pathogen-free facility. Experiments were performed in accordance to the guidelines set forth by Institutional Animal Care and Use Committee at Columbia University Medical Center.

Analysis of VWF expression and function

Detection and/or measurement of murine VWF A1-A2-A3 domain transcripts, plasma VWF antigen levels, functional factor VIII levels, and multimer pattern were performed as previously described.[27-30]

Platelet adhesion in flow

A parallel-plate flow chamber was used to assess platelet attachment and translocation on surface-immobilized plasma VWF or recombinant VWF-A1 protein.[27] Generation and purification of recombinant proteins were performed as previously described.[20,26] Citrated whole blood (150 µl) collected via cardiac puncture from anesthetized WT and mutant VWF mice or from healthy human volunteers (venipuncture) was perfused over the immobilized substrates at wall shear rates ranging from 100 s^{-1} to 1,600 s^{-1} for 2 min, followed by washing with Tyrode's buffer. The number of platelets attached per unit area and translocation velocities were determined by off-line analysis. For inhibition studies, OS1 peptide was generated and purified as previously described.[31] The inhibitor was added to 1 ml of citrated whole blood 5 minutes prior to perfusing over surface-immobilized substrates.

Platelet aggregation

The ability of ristocetin (Chronolog Corporation) to aggregate human platelets in plasma obtained from healthy volunteers or VWF mutant mice was assessed using a Lumi-

Aggregometer (model 540 VS, Chronolog Corporation).[32] In brief, citrated whole blood obtained by cardiac puncture from anesthetized mice or collected via venipuncture from healthy volunteers was centrifuged to obtain platelet poor plasma (PPP). Subsequently, lyophilized human platelets (Bio/Data Corporation) reconstituted in TBS were added to plasma at a 4:1 ratio (v/v) and a baseline obtained for 2 minutes prior to adding ristocetin (1.25 mg/ml). Aggregation (1,200 rpm, 37°C) was allowed to proceed for 6 min. Results are reported as maximum percent change in light transmittance from baseline with TBS used as a reference. For inhibition studies, platelet / PPP mixture was incubated with OS1 peptide (0.1 µg/ml to 5 µg/ml) for 5 min prior to the addition of ristocetin.

***In vivo* thrombus formation.**

Administration of anesthesia, insertion of vascular catheters, fluorescent labeling of platelets, and surgical preparation of the cremaster muscle have been previously described.[27,32] A pulsed nitrogen dye laser was used to induce arteriole injury in the cremaster muscle of anesthetized 8-12 week old animals. Mouse or human platelet-vessel wall interactions were visualized by fluorescen ce microscopy. Human platelets were administered by continuous infusion (700,000/µl at 25 µl/min) through a catheter placed in the ipsilateral femoral artery 2 minutes before and during laser-induced injury. For inhibition studies, 20 µg of OS1 peptide in 100 µl of saline was administered i.v. 5 min prior to the administration of human platelets. The extent of thrombus formation was assessed for 2 min post injury and the area (μm^2) of coverage.

Tail bleeding assay

Bleeding times were measured in 8-week old mice after amputating 1 cm of the tail tip and then placing the tail in a physiological saline solution (37°C) as previously described.[27]

Microsphere tethering frequency

The rate of complex formation was evaluated by measuring the frequency of tethering events between surface-immobilized mouse platelets and microspheres coated with a low site density of recombinant WT or mutant VWF-A1.[20,21] This was determined by observing the number of beads that paused, but did not translocate, at wall shear rates ranging from 10 s^{-1} to 300 s^{-1}. This value was then normalized by dividing the number of beads that formed transient tethers by the number of non-interacting beads transported across the field of view in the focal plane of the immobilized platelet substrate. Estimation of the amount of VWF-A1 coupled to beads was determined using a calibrated microbead system (Flow Cytometry Standards) following manufacturer's instructions. The site density of VWF-A1 on beads was estimated to be ~35 sites/μm^2.

Dissociation rate constants of transient tethers

The duration of transient tethers was estimated for VWF-A1-coated microspheres interacting with surface-immobilized platelets at wall shear stresses ranging from 0. 5 to 3.0 dyn/cm^2. [20,21] Only one tethering event per bead was counted during the observation

period. The duration of these interactions was measured by recording images at a frame rate of 235 frames per second using 60X DIC objective (oil immersion). A total of 30–50 interact pause times for each wall shear stress was recorded. Dissociation rate constants were determined by plotting the natural log of the number of VWF-A1–coated microspheres that interacted as a function of time after the initiation of tethering. The slope of the line = $-k_{off}$. The force acting on the tether bond was calculated from force balance equations (bead radius of 3.5μm) satisfied with a tether angle θ of 57.2 degrees.[20,21]

Statistical analyses

Details for the calculation of maximum likelihood estimates (MLEs) for the off-rates (k_{off}) and Bell model parameters (k^0_{off}, σ) can be found in supplemental Methods. Statistical analysis of all other data was determined using unpaired Student's *t*-test (GraphPad Prism software). Values were considered significant at $P < 0.05$.

Results

Structural and functional changes associated with I1309V and R1326H mutations

To determine the interplay between known contact surfaces and to establish the role that the biophysical properties of the GPIbα–VWF-A1 bond play in regulating platelet–VWF interactions, we chose mutations within the major or minor contact interfaces of the murine A1 domain that enhance (I1309V) or disrupt (R1326H) binding. The I1309V mutation is known to cause type 2B VWD,[33] while the R1326H substitution impairs interactions with mouse GPIbα.[27] Interestingly, several mammalian species including humans have a histidine in lieu of arginine at position 1326 within the A1 domain.[34] Thus, murine VWF is ideal for determining how this particular amino acid substitution alters the biophysical properties of the GPIbα–VWF-A1 bond and its ability to support hemostasis and thrombosis. Models of WT and mutant murine complexes were built to better understand the effect of the mutations on binding (Figure 1A). Although crystal structure analyses have yet to identify the exact mechanism by which the I1309V mutation augments adhesion,[9,13] it is located in the α1-β2 loop adjacent to the type 2B mutation R1306Q.[9,10] The latter mutation is believed to result in a local conformational change with a re-positioning of residues Q1311 and R1334 that reinforce interactions with human GPIbα.[9] Figure 1B illustrates the position of residue 1309 in the context of the complex formed with murine GPIbα and the augmentation in binding that occurs upon re-positioning of residues Q1311 and R1334.

To understand how these mutations affect adhesion under flow conditions, we generated recombinant murine VWF-A1 (rVWF-A1) proteins containing the R1326H

and I1309V substitutions and determined their ability to support mouse platelet interactions when surface-immobilized in a parallel plate flow system.[27] The R1326H mutation impaired mouse platelet accumulation and increased translocation velocity ~13-fold as compared to WT rVWF-A1 (Figure 1C-D). In contrast, the I1309V mutation decreased translocation velocity ~5-fold and greatly augmented platelet accumulation. Strikingly, rVWF–A1 containing both amino acid substitutions yielded an adhesive phenotype comparable to WT.

I1309V and R1326H mutations differentially alter bond formation and dissociation

To determine whether the biophysical properties of rVWF-A1 expressing both mutations truly reflect that of the WT complex, we analyzed the formation and dissociation of transient adhesive events, known as tether bonds, that occur when flowing rVWF-A1–coated microspheres transiently interact with GPIbα expressed on surface-immobilized mouse platelets.[20,21] On-rate was determined by evaluating the frequency with which microspheres interacted with surface-immobilized mouse platelets at various wall shear rates. Whereas the I1309V mutation enhanced the rate of association ~3.5–fold, this was abolished when combined with the R1326H substitution (Figure 2A). In fact, murine rVWF-A1 possessing the double mutation displayed a rate of association that more closely resembled the WT complex with a maximal tethering frequency at a wall shear rate of 85 s^{-1}.

The effects of the mutations on the kinetics of dissociation (k_{off}) were determined measuring the lifetime of tether bonds and their response to an applied force.[20,21] We

previously showed the utility of this system for assessing the biophysical properties of the interaction between human GPIbα and rVWF-A1. Moreover, the use of microspheres with a uniform size and shape permits the calculation of the amount of shear force acting on the tether bond. As previously observed for the human complex, the distribution of interaction times indicated that the majority of WT and mutant tether bonds fit a straight line, the regressed slope of which corresponded to $-k_{off}$ (Figure 2B-E). In addition, the rate of dissociation behaved in accordance with the equation of Bell, which states that $k_{off} = k^0_{off} exp(\sigma F_b/kT)$, where F_b is the applied force, k^0_{off} is the dissociation rate constant in the absence of force, kT is the thermal energy, and σ (reactive compliance) relates the sensitivity of bond off-rate to an applied force.[35] The larger the values for k^0_{off} and σ, the shorter the bond lifetime ($1/ k^0_{off}$) and the more prone the receptor–ligand interaction is to force-driven dissociation, respectively. Maximum likelihood estimates (MLE) of the kinetics of GPIbα–VWF-A1 interactions and their subsequent fit to the Bell equation were performed.[36] Regression analyses of these simulations fit the data at bond forces ranging from 36 pN to 217 pN and thus permitted the determination of k^0_{off} and σ (Figure 2F and Table 1). Whereas the major effect of the I1309V substitution was to prolong the lifetime of the tether bond (6-fold), R1326H shortened its duration (2.5-fold). However, the kinetic (k^0_{off}) and mechanical (σ) properties of rVWF-A1 bearing both mutations were nearly identical to that of the native complex.

Hemostatic and thrombotic properties of murine VWF possessing mutant A1 domains

To determine whether the predictions based on biophysical studies truly have biological relevance, we generated knock-in mice that express either the R1326H (VWF ^{R1326H}) mutation alone[27] or in combination with I1309V (VWF $^{I1309V,\ R1326H}$) (supplemental Figure 1A-C). VWF gene transcription, multimer pattern, antigen levels as well as factor VIII function and platelet counts were similar to WT littermates (supplemental Figure 1D-H). Consistent with the reduction in bond lifetime and impaired adhesion, animals expressing the R1326H mutation had prolonged tail bleeding times and a diminished capacity to form arterial thrombi (Figure 3A-B). In fact, VWF ^{R1326H} mice possessed a phenotype similar to that observed for mice lacking this plasma protein (VWF ^{KO}). Remarkably, the additional incorporation of the I1309V mutation corrected the observed perturbations in platelet–VWF interactions. Not only did VWF-A1 double mutant animals have hemostatic properties similar to WT littermates, but also laser-induced thrombi were comparable in size to mice possessing the WT plasma protein (Figure 3A-B). Direct evidence that plasma VWF $^{I1309V,\ R1326H}$ has adhesive properties equivalent to its WT counterpart is demonstrated by its ability to support mouse platelet accumulation and translocation velocities at similar levels (Figure 3C-D). This was not the case for plasma VWF ^{R1326H} which impaired platelet adhesion and yielded a ~3-fold increase in translocation velocity. These data support a close association between the lifetime of the GPIbα–VWF-A1 bond and the ability of these hemostatic elements to support critical biological processes.

Targeting the major binding interface between human GPIbα and VWF-A1

Given the importance of the major contact site in supporting mouse platelet–VWF interactions *in vivo*, we next explored the therapeutic utility of targeting this region in the human complex. This was accomplished by using a novel cyclic peptide, termed OS1, which was isolated from a cysteine-constrained phage display library.[31] It interacts with the curved concave face of the GPIbα leucine-rich repeat,[37] stabilizing a conformation of a regulatory loop known as the β-switch[10] so that it prevents the formation of electrostatic interactions essential for binding to the VWF-A1 domain (Figure 4A). However, the effect of OS1 is limited to human GPIbα as demonstrated by its inability to reduce mouse platelet–VWF interactions *in vitro* and *in vivo* (Figure 4B-C). In contrast, incubation of whole blood from healthy volunteers with the inhibitor not only limited platelet accumulation on surface-immobilized human rVWF-A1 protein, but also impaired ristocetin-induced platelet aggregation in a dose dependent manner (Figure 4D-E).

To directly test the ability of OS1 to prevent human platelet-mediated arterial thrombosis, we generated an animal in which the majority of the murine A1 domain was replaced with its human counterpart (supplemental Figure 2A-B). VWF gene transcription, multimer pattern, antigen levels and platelet counts in VWF ^{HA1} mice were similar to WT littermate controls (supplemental Figure 2C-F). In addition, animals containing the human VWF-A1 domain manifested impaired platelet–vessel wall interactions that resulted in a prolongation in tail bleeding time as well as a reduction in thrombus size in laser-injured arterioles (Figure 5A-B). Consistent with these observations was the inability of surface-immobilized plasma VWF ^{HA1} to support mouse platelet accumulation in flow (Figure 5C). In the presence of human platelets, however,

VWF ^{HA1} mice formed large and often occlusive thrombi in laser-injured arterioles of nearly identical size to that observed in their VWF ^{R1326H} counterparts (Figure 5D). Accumulation of human platelets on surface-immobilized plasma VWF from either animal was also comparable (Figure 5E). Yet, only plasma VWF from mice possessing the human VWF-A1 domain supported ristocetin-induced platelet agglutination / aggregation of human platelets demonstrating that the R1326H mutation in murine VWF-A1 was not sufficient to support this process (Figure 5F). Importantly, the OS1 peptide was able to impair human platelet accumulation on surface-immobilized plasma VWF ^{HA1} and inhibited ristocetin-induced platelet agglutination / aggregation (Figure 6A-B). Moreover, human platelet-mediated thrombus formation in arterioles of VWF ^{HA1} mice was reduced by >80% in the presence of the inhibitor (Figure 6C). The data demonstrate the potential therapeutic utility in targeting the major contact interface formed between the human GPIbα–VWF-A1 complex.

Discussion

Detailed structural and biophysical analyses of small regions of contact between GPIbα and VWF-A1 have yielded tremendous insight into the relationship between force-lifetime-and-chemistry of an interaction critical for supporting hemostasis and thrombosis. Here, we have taken a unique approach to better understand the role that the kinetic properties of the contact surfaces formed between this receptor–ligand pair play in supporting these biologically relevant processes. By generating animals with mutations contained within the major and minor binding sites of murine VWF-A1 that either reduce or enhance attachment to GPIbα, we provide the first *in vivo* evidence that bond lifetime does play an important role in regulating platelet–VWF interactions at sites of arterial injury.

To determine whether data obtained using a murine-based system were applicable to the human receptor–ligand pair, we first measured the kinetic properties of the murine GPIbα–VWF-A1 bond and its response to an applied force. Values for the intrinsic off-rate were similar between the species (k^0_{off} values of 3.05 ± 0.55 s^{-1} and 3.45 ± 0.37 s^{-1} for the mouse and human complex, respectively). However, the reactive compliance (σ) for the WT murine complex was ~1.5-fold higher than for its human counterpart (0.028 ± 0.001 nm versus 0.018 ± 0.002 nm, respectively), suggesting that the interaction between the murine receptor–ligand pair may be slightly more prone to dissociate upon the application of hydrodynamic force. The effects of the I1309V substitution mirrored that of the human rVWF-A1 mutant[20], including the reduced requirement for shear flow to promote GPIbα interactions with VWF-A1 and a prolongation in bond lifetime.

Surprisingly, the observed alterations in adhesion did not persist when this mutation was combined with R1326H. In fact, the biophysical properties of the double mutant bond more closely resembled that of the native complex. These observations led us to predict that murine plasma VWF $^{I1309V,\ R1326H}$ should possess hemostatic and thrombotic properties similar to the native plasma protein if bond lifetime plays an important role in these processes. This was borne out by the fact that I1309V, R1326H double knock-in mice had tail bleeding times and formed arterial thrombi of similar size to that observed for WT littermates. Based on these observations we conclude that the major and minor contact interfaces not only contribute to a biophysical signature well suited for supporting platelet–VWF interactions under the hydrodynamic conditions encountered in the arterial circulation, but also that they must be maintained within strict limits in order to optimize platelet accumulation at sites of vascular injury.

Although the precise mechanism(s) by which the I1309V mutation augments binding remains controversial,[9,13] its pronounced effects on the biophysical properties of the murine GPIbα–VWF-A1 bond made it suitable for gaining insight into the relationship between bond lifetime and the requirement for shear flow to initiate platelet attachment to VWF. It is well known that the application of a specific level of shear is essential to achieve optimal adhesion between GPIbα and VWF-A1 (termed the shear threshold effect).[20] Shear-induced forces are thought to influence the GPIbα–VWF-A1 bond in two ways. As the applied force increases from low levels, the bond lifetime increases until it is of sufficient duration to promote effective interactions between platelets and VWF (termed a catch bond).[38-40] It is only when force exceeds the critical value does the lifetime shorten and the bond ultimately rupture (termed a slip bond) in

accordance with Bell's model.[35] However, this concept has been challenged in a study suggesting that the shear threshold effect may be due to a transition of a slip bond from a low to high affinity state in response to a force-induced conformation change in the complex.[41] Despite these conflicting views, our data suggest that the ability of the I1309V mutation to prolong the lifetime of the GPIbα–VWF-A1 bond beyond that of the native complex is essential for promoting platelet–VWF interactions at low flow states. Moreover, the process is reliant on the biophysical properties of the major contact interface. In the presence of the R1326H substitution, the I1039V mutation could no longer abolish the requirement for shear flow to support the tethering of murine rVWF-A1 coated beads to mouse GPIbα, nor slow mouse platelet translocation velocities and augment platelet attachment to surface immobilized VWF-A1 containing the double mutation.

It is important to note that the ability to prolong the lifetime of the GPIbα–VWF-A1 bond is not unique to type 2B mutations as it has also been reported for snake venoms. This is best exemplified by the ability of botrocetin, a component of *Bothrops jararaca* venom, to promote platelet–VWF aggregation in plasma as well as contribute to the loss of VWF multimers and platelets from the blood.[42] Interestingly, we have shown that the major effect of botrocetin is to increase the bond lifetime two-fold for both human and mouse complexes without affecting the on-rate.[26] This did not involve allosteric changes in GPIbα or VWF-A1, but relied on the ability of the venom protein to form a biological clasp that prolonged their embrace. These results further support our current observations that the lifetime of the GPIbα–VWF-A1 bond contributes significantly to promoting effective platelet–VWF interactions at sites of arterial injury.

There has been much speculation on whether one or both of the identified binding surfaces between GPIbα and VWF-A1 could be targets for the prevention or treatment of thrombosis.[43] Our current study helps clarify this issue. We demonstrate that a cyclic peptide (OS1) proven to alter the conformation of GPIbα so that is incapable of forming several key interactions with the major binding interface of VWF-A1 significantly reduced human platelet-mediated thrombus formation in laser-injured arterioles of VWF ^{HA1} mice. Thus, the development of such agents that can alter specific interactions between this receptor–ligand pair offers a powerful approach to reducing arterial thrombosis.

In summary, animals bearing specific mutations in a protein critical to promoting hemostasis and thrombosis help to establish an essential link between kinetic measurements of a receptor-ligand bond and their overall significance to a biologically relevant process. In addition, our data shed new light on the cooperation between the two distinct GPIbα binding sites within VWF-A1 in generating a biophysical signature ideally suited for supporting platelet–VWF interactions to sites of arterial injury. Insights into how the interaction between a receptor–ligand pair can be altered by manipulating the kinetics of a receptor-ligand interaction are relevant to the development of therapies aimed at either disrupting or correcting disorders related to cell adhesion.

Acknowledgements

We thank Aychyn C. Huang and Jeffrey S. Jhang for performing factor VIII function analysis, Gray Shaw for supplying the OS1 peptide, and Ian Laurenzi for performing the analysis of tether bond formation. We are grateful to Barry Coller and Michael Rosen for critical review of the manuscript. This research is supported by National Institute of Health grants HL103989 and HL097971. The authors have no competing financial interests.

Authorship contributions

T.G.D. conceived the study, supervised the project, conducted experiments, and wrote the manuscript. J.C. generated VWF mutant mice and conducted experiments. H.Z. and X.L.Z. performed experiments and J.E. generated atomic models of the murine GPIbα–VWF complex. I.J.L. conducted MC simulations and statistical analysis of the biophysical data.

References

1. Ruggeri ZM, Orje JN, Habermann R, Federici AB, Reininger AJ. Activation-independent platelet adhesion and aggregation under elevated shear stress. *Blood*. 2006;108(6):1903-1910.

2. Sakariassen KS, Bolhuis PA, Sixma JJ. Human blood platelet adhesion to artery subendothelium is mediated by factor VIII-Von Willebrand factor bound to the subendothelium. *Nature*. 1979;279(5714):636-638.

3. Nichols WC, Ginsburg D. von Willebrand disease. *Medicine (Baltimore).* 1997;76(1):1-20.

4. Sadler JE. New concepts in von Willebrand disease. *Annu. Rev. Med*. 2005;56:173-191.

5. Cruz MA, Diacovo TG, Emsley J, Liddington R, Handin RI. Mapping the glycoprotein Ib-binding site in the von Willebrand factor A1 domain. *J. Biol. Chem*. 2000;275(25):19098-19105.

6. Piétu G, Meulien P, Cherel G, et al. Production in Escherichia coli of a biologically active subfragment of von Willebrand factor corresponding to the platelet glycoprotein Ib, collagen and heparin binding domains. *Biochem. Biophys. Res. Commun*. 1989;164(3):1339-1347.

7. Savage B, Saldivar E, Ruggeri ZM. Initiation of platelet adhesion by arrest onto fibrinogen or translocation on von Willebrand factor. *Cell*. 1996;84(2):289-297.

8. Sugimoto M, Ricca G, Hrinda ME, et al. Functional modulation of the isolated

glycoprotein Ib binding domain of von Willebrand factor expressed in Escherichia coli. *Biochemistry*. 1991;30(21):5202-5209.

9. Dumas JJ, Kumar R, McDonagh T, et al. Crystal structure of the wild-type von Willebrand factor A1-glycoprotein Ibalpha complex reveals conformation differences with a complex bearing von Willebrand disease mutations. *J. Biol. Chem.* 2004;279(22):23327-23334.

10. Huizinga EG, Tsuji S, Romijn RA, et al. Structures of glycoprotein Ibalpha and its complex with von Willebrand factor A1 domain. *Science*. 2002;297(5584):1176-1179.

11. Emsley J, Cruz M, Handin R, Liddington R. Crystal structure of the von Willebrand Factor A1 domain and implications for the binding of platelet glycoprotein Ib. *J. Biol. Chem.* 1998;273(17):10396-10401.

12. Fukuda K, Doggett TA, Bankston LA, Cruz MA, Diacovo TG, Liddington RC. Structural basis of von Willebrand factor activation by the snake toxin botrocetin. *Structure*. 2002;10(7):943-950.

13. Blenner MA, Dong X, Springer TA. Towards the Structural Basis of Regulation of von Willebrand Factor Binding to Glycoprotein Ib. *J. Biol. Chem*. 2014;289(9):5565-5579

14. Lenting PJ, Pegon JN, Groot E, de Groot PG. Regulation of von Willebrand factor-platelet interactions. *Thromb Haemost*. 2010;104(3):449-455.

15. Ulrichts H, Udvardy M, Lenting PJ, et al. Shielding of the A1 domain by the D'D3 domains of von Willebrand factor modulates its interaction with platelet glycoprotein Ib-IX-V. *J Biol Chem*. 2006;281(8):4699-4707.

16. Hulstein JJ, Lenting PJ, de Laat B, Derksen RH, Fijnheer R, de Groot PG. beta2-Glycoprotein I inhibits von Willebrand factor dependent platelet adhesion and aggregation. *Blood*. 2007; 110(5):1483–1491.

17. Dong JF, Berndt MC, Schade A, McIntire LV, Andrews RK, Lopez JA. Ristocetin-dependent, but not botrocetin-dependent, binding of von Willebrand factor to the platelet glycoprotein Ib-IX-V complex correlates with shear-dependent interactions. *Blood*. 2001;97(1):162-168.

18. Schneider SW, Nuschele S, Wixforth A, et al. Shear-induced unfolding triggers adhesion of von Willebrand factor fibers. *Proc Natl Acad Sci USA* 2007; 104(19):7899–7903.

19. Arya M, Kolomeisky AB, Romo GM, Cruz MA, Lopez JA, Anvari B. Dynamic force spectroscopy of glycoprotein Ib-IX and von Willebrand factor. *Biophys J*. 2005;88(6):4391-4401.

20. Doggett TA, Girdhar G, Lawshé A, et al. Selectin-like kinetics and biomechanics promote rapid platelet adhesion in flow: the GPIbα-vWF tether bond. *Biophys J*. 2002;83(1):194-205.

21. Doggett TA, Girdhar G, Lawshe A, et al. Alterations in the intrinsic properties of the GPIb alpha – vWF tether bond define the kinetics of the platelet-type von Willebrand disease mutation, G233V. *Blood*. 2003;102(1):152-160.

22. Kumar RA, Dong JF, Thaggard JA, Cruz MA, Lopez JA, McIntire LV. Kinetics of GPIbα–vWF-A1 tether bond under flow: effect of GPIbα mutations on the association and dissociation rates. *Biophys J*. 2003;85(6):4099-4109.

23. Dufrêne YF, Evans E, Engel A, Helenius J, Gaub HE, Müller DJ. Five challenges to bringing single-molecule force spectroscopy into living cells. *Nat Methods*. 2011;8(2):123-127.

24. Neuman KC, Nagy A. Single-molecule force spectroscopy: optical tweezers, magnetic tweezers and atomic force microscopy. *Nat Methods*. 2008;5(6):491-505.

25. Weisel JW, Shuman H, Litvinov RI. Protein-protein unbinding induced by force: single-molecule studies. *Curr Opin Struct Biol*. 2003;13(2):227-235.

26. Fukuda K, Doggett T, Laurenzi IJ, Liddington RC, Diacovo TG. The snake venom protein botrocetin acts as a biological brace to promote dysfunctional platelet aggregation. *Nat Struct Mol Biol*. 2005;12(2):152-159.

27. Chen J, Tan K, Zhou H, et al. Modifying murine von Willebrand factor A1 domain for in vivo assessment of human platelet therapies. *Nat Biotechnol*. 2008;26(1):114-119.

28. Cao WJ, Krishnaswamy S, Camire RM, Lenting PJ, Zheng XL. Factor VIII accelerates proteolytic cleavage of von Willebrand factor by ADAMTS13. *Proc Natl Acad Sci U S A*. 2008;105(21):7416-7421.

29. Laje P, Shang D, Cao W, et al. Correction of murine ADAMTS13 deficiency by hematopoietic progenitor cell-mediated gene therapy. *Blood*. 2009;113(10):2172-2180.

30. Niiya M, Endo M, Shang D, et al. Correction of ADAMTS13 deficiency by in utero gene transfer of lentiviral vector encoding ADAMTS13 genes. *Mol Ther*. 2009;17(1):34-41.

31. Benard SA, Smith TM, Cunningham K, et al. Identification of peptide antagonists to glycoprotein Ibalpha that selectively inhibit von Willebrand factor dependent platelet aggregation. *Biochemistry*. 2008;47(16):4674-4682.

32. Magallon J, Tan K, Zhao H, Tronik-Le Roux D, Liddington RC, Diacovo TG. Humanized mouse model of thrombosis is predictive of the clinical efficacy of antiplatelet agents. *Circulation*. 2011;123(3):319-326.

33. Federici AB, Mannucci PM, Stabile F, et al. A type 2b von Willebrand disease mutation (Ile546-->Val) associated with an unusual phenotype. *Thromb Haemost.* 1997;78(3):1132-1137.

34. Jenkins PV, Pasi KJ, Perkins SJ. Molecular modeling of ligand and mutation sites of the type A domains of human von Willebrand factor and their relevance to von Willebrand's disease. *Blood*. 1998;91(6):2032-2044.

35. Bell GI. Models for the specific adhesion of cells to cells. *Science.* 1978;200(4342):618-627.

36. Uz B, Arslan E, Laurenzi IJ. Maximum likelihood estimation of the kinetics of receptor-mediated adhesion. *J. Theo. Bio*. 2010;262 (3):478-448.

37. McEwan PA, Andrews RK, Emsley J. Glycoprotein Ibα inhibitor complex structure reveals a combined steric and allosteric mechanism of von Willebrand factor antagonism. *Blood*. 2009;114(23):4883-4885.

38. Marshall BT, Long M, Piper JW, Yago T, McEver RP, Zhu C. Direct observation of catch bonds involving cell-adhesion molecules. *Nature.* 2003;423(6936):190-193.

39. Thomas WE. Mechanochemistry of receptor-ligand bonds. *Curr Opin Struct Biol*. 2009;19(1):50-55.

40. Yago T, Lou J, Wu T, et al. Platelet glycoprotein Ibalpha forms catch bonds with human WT vWF but not with type 2B von Willebrand disease vWF. *J Clin Invest.* 2008;118(9):3195-3207.

41. Kim J, Zhang CZ, Zhang X, Springer TA. A mechanically stabilized receptor-ligand flex-bond important in the vasculature. *Nature.* 2010;466(7309):992-995.

42. Sanders WE, Read MS, Reddick RL, Garris JB, Brinkhous KM. Thrombotic thrombocytopenia with von Willebrand factor deficiency induced by botrocetin. An animal model. *Lab Invest*. 1988;59(4):443−452.

43. Sadler JE. Biomedicine. Contact--how platelets touch von Willebrand factor. *Science*. 2002;297(5584):1128-1129.

Figure legends

Figure 1. I1309V mutation rescues the defect in platelet adhesion associated with the R1326H mutation. (A and B) Proposed models for the WT (A) and double mutant (I1306V, R1326H) (B) murine VWF-A1 domains (gray) in complex with murine GPIbα (cyan). The β-switch hairpin loop of GPIbαis shown in green and key side chains involved in forming the interface are shown in stick. Zooms reveal details of the electrostatic interactions that may be altered by the mutations R1326H and I1309V, respectively. (C and D) Accumulation (C) and translocation velocity (wall shear rate of 1,600 s^{-1}) (D) of mouse platelets on surface-immobilized recombinant murine VWF-A1 proteins. Platelet attachment and their subsequent motion were digitally recorded on an inverted Nikon microscope (Eclipse TE2000) with a plan 10X or 20X objective, respectively. The number of platelets attached per unit area and translocation velocities were determined by off-line analysis (Image-Pro Plus, Media Cybernetics). Data are representative of the mean of three separate experiments performed in triplicate (± standard deviation).

Figure 2. Kinetics of tether bond formation and dissociation. (A) Frequency of transient adhesive interactions between microspheres coated with recombinant VWF-A1 protein and surface-immobilized mouse platelets (wall shear rates 10 s^{-1} to 300 s^{-1}). (B–E) Representative graphs depicting the distribution of pause times for more than 30 individual transiently tethered VWF-A1 coated microspheres at the indicated wall shear

stresses. The dissociation rate constant (k_{off}) is the negative slope of the linear regression through the experimental data. (F) Effect of force on the GPIbα–VWF-A1 tether bond as a function of k_{off}. pN, piconewtons. Tethering frequency and estimation of k_{off} values for VWF-A1 coated microspheres transiently interacting with surface-immobilized platelets were determined by recording digital images with a Nikon 10X plan or 60X DIC objective (oil immersion) at frame rates of 30fps or 235 fps, respectively (Speed Vision Technologies, San Diego, CA). Results represent the mean ± standard deviation.

Figure 3. Hemostatic and thrombotic properties of plasma VWF $^{I1309V, R1326H}$. (A) Tail bleeding times for WT, VWF ^{KO}, VWF ^{R1326H}, and VWF $^{I1309V, R1326H}$ mice. Each point represents one individual animal; lines show the mean of each group. (B) Thrombus formation in laser-injured arterioles of WT and VWF mutant mice (n = 7 mice per genotype; 1 arteriole per mouse). Platelet-vessel wall interactions were visualized through a 20X water-immersion objective (Olympus LUMPlanFl, 0.5 NA) using a Zeiss Axiotech Vario microscope equipped with a Yokogawa CSU-22 spinning disk confocal scanner, iXON EM camera, and 561 nm laser line to detect rhodamine-labeled mouse platelets (Revolution XD, Andor™ Technology). The extent of thrombus formation was assessed for 2 min post injury and the area (μm^2) of coverage determined by off-line analysis (Image IQ, Andor™ Technology and Image-Pro Plus, Media Cybernetics). (C and D) Accumulation (C) and translocation velocities (wall shear rate 1,600 s^{-1}) (D) of mouse platelets on surface-immobilized WT or mutant plasma VWF at the indicated wall shear rates (n = 3 separate experiments). Images were obtained using a CCD camera and analyzed using Image-Pro Plus. Data are the mean ± standard deviation, ns = not

significant ($P > 0.05$). *$P < 0.05$ and **$P < 0.0001$ relative to control.

Figure 4. Disrupting the major contact interface with the allosteric inhibitor OS1 limits human platelet–VWF interactions. (A) Ribbon representation of the human GPIbα–VWF-A1–OS1 ternary complex (upper panel). The change in R-loop conformation imposed upon OS1 cyclic peptide (purple) binding to GPIbα is depicted in the panel on the right. (B and C) OS1 peptide is specific for human GPIbα. (B) Accumulation of mouse platelets on surface-immobilized murine rVWF-A1 protein (wall shear rate of 1,600 s^{-1}) in the absence of presence of the inhibitor (n=3). Images were obtained with a CCD camera and analyzed using Image-Pro Plus (C) Thrombus formation in laser injured arterioles of WT mice animals that received an infusion of vehicle control or OS1 peptide (n = 7 mice per treatment condition; 1 arteriole per mouse). Fluorescent imagines were obtained using a 20X water-immersion objective, a Yokogawa CSU-22 spinning disk confocal scanner, and a 561 nm laser line to detect rhodamine-labeled mouse platelets. (D) Accumulation of human platelets on surface-immobilized human VWF-A1 protein (wall shear rate of 1,600 s^{-1}) in the absence or presence of the inhibitor (n=3). Images were obtained using a CCD camera and analyzed using Image-Pro Plus. (E) Ristocetin-induced aggregation of human platelets in the presence of human plasma. Data are the mean ± standard deviation, ns = not significant ($P > 0.05$).

Figure 5. Hemostatic and thrombotic properties of plasma VWF ^{HA1}. (A) Tail bleeding times for WT, VWF ^{R1326H}, and VWF ^{HA1} mice. Each point represents one individual animal; lines show the mean of each group. (B) Thrombus formation in laser-injured arterioles of WT and VWF mutant mice (n = 7 mice per genotype; 1 arteriole per animal). Fluorescent imagines were obtained using a 20X water-immersion objective, a Yokogawa CSU-22 spinning disk confocal scanner, and a 561 nm laser line to detect rhodamine-labeled mouse platelets. (C) Accumulation of mouse platelets on surface-immobilized WT or mutant plasma VWF at a wall shear rate of 1,600 s^{-1} (n = 3). Images were obtained using a CCD camera and analyzed using Image-Pro Plus. (D) Human platelet mediated thrombus formation in laser injured arterioles of WT or VWF mutant animals (n = 7 mice per genotype; 1 arteriole per animal). A 488 nm laser line was used to detect BCECF-labeled human platelets. (E) Accumulation of human platelets on surface-immobilized WT or mutant plasma VWF at a wall shear rate of 1,600 s^{-1} (n = 3). (F) Representative plot depicting the extent of ristocetin-induced agglutination / aggregation of lyophilized human platelets in plasma from human volunteers or VWF mutant animals (n = 2 experiments performed in duplicate). Data are the mean ± standard deviation, ns = not significant ($P > 0.05$).

Figure 6. Disrupting the major contact interface between human GPIbα and VWF ^{HA1} reduces arterial thrombus formation. (A and B) Effect of the OS1 peptide on human platelet accumulation on surface-immobilized plasma VWF ^{HA1} (wall shear rate of 1,600 s^{-1}; n=3) (A) and ristocetin-induced human platelet aggregation in the presence of plasma from VWF ^{HA1} animals (B; n=2). Images were obtained using a CCD camera and

analyzed using Image-Pro Plus. (C) Effect of OS1 peptide on human platelet-mediated thrombus formation in arterioles of VWF ^{HA1} mice (n = 7 mice per genotype; 1 arteriole per animal). A 488 nm laser line was used to detect BCECF-labeled human platelets. Data are the mean ± standard deviation. $^{**}P < 0.001$ relative to control.

Figure 1

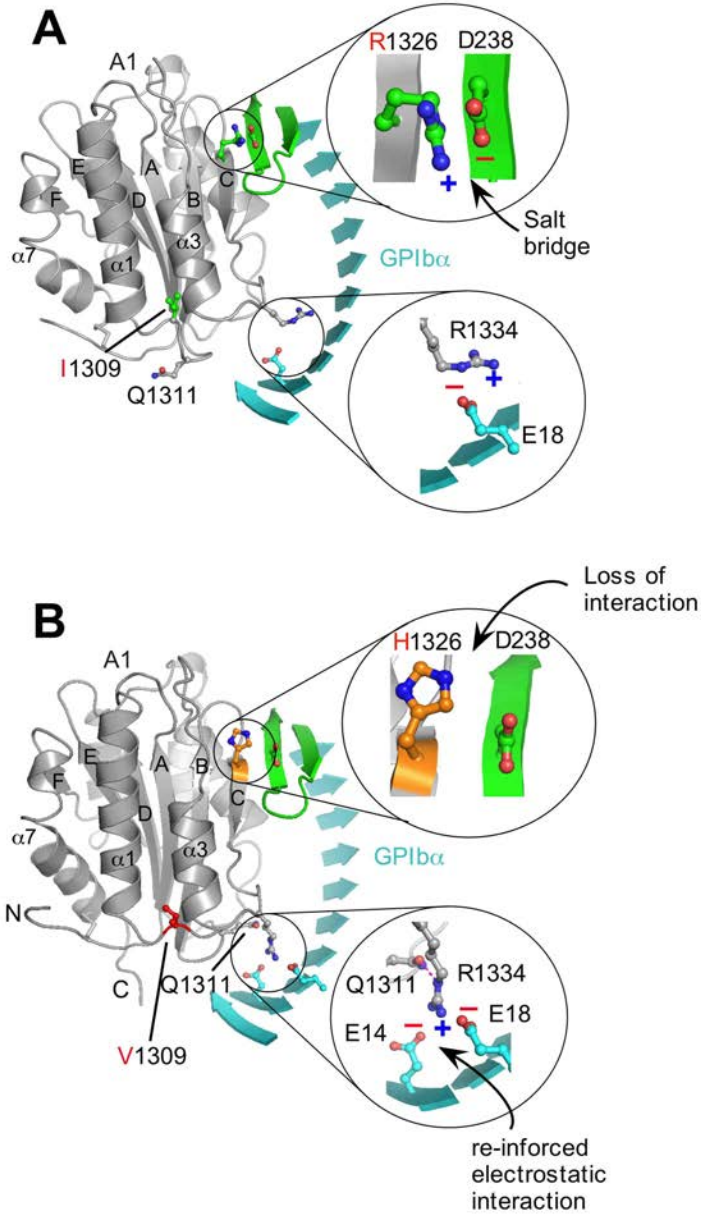
A
A1
R1326
D238
Salt bridge
GPIbα
R1334
E18
I1309
Q1311
B
Loss of interaction
H1326
D238
GPIbα
N
C
Q1311
V1309
R1334
E18
E14
re-inforced electrostatic interaction

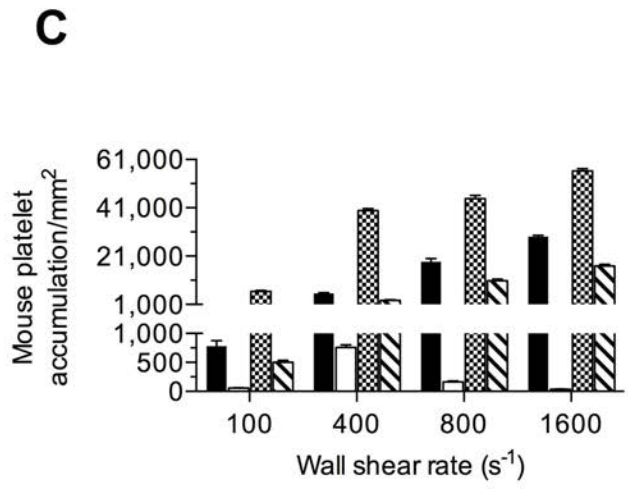
C
Mouse platelet accumulation/mm²
61,000
41,000
21,000
1,000
1,000
500
0
100
400
800
1600
Wall shear rate (s⁻¹)


rVWF–A1 (WT)
rVWF–A1 (R1326H)
rVWF–A1 (I1309V)
rVWF–A1 (I1309V, R1326H)

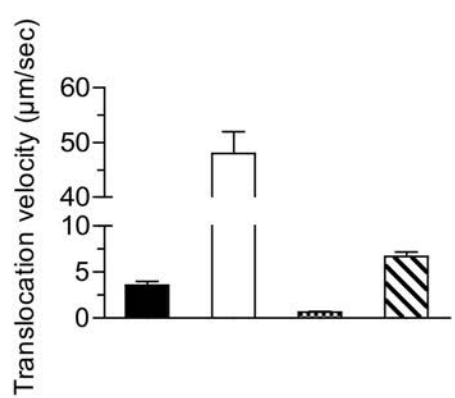
D
Translocation velocity (μm/sec)
60
50
40
10
5
0

Figure 2

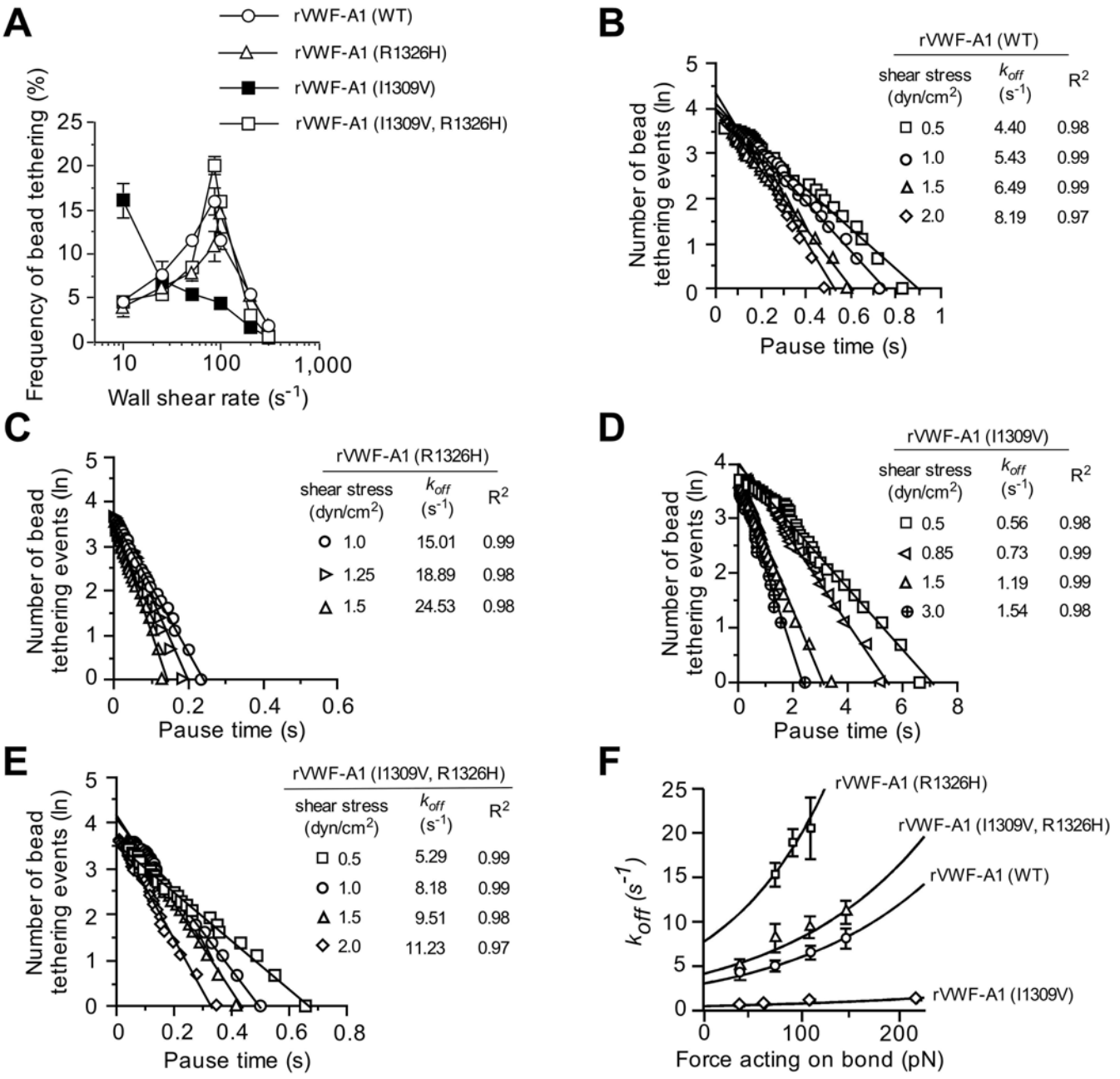
A
rVWF-A1 (WT)
rVWF-A1 (R1326H)
rVWF-A1 (I1309V)
rVWF-A1 (I1309V, R1326H)
Frequency of bead tethering (%)
Wall shear rate (s-1)
B
rVWF-A1 (WT)
shear stress (dyn/cm2) koff (s-1) R2
0.5 4.40 0.98
1.0 5.43 0.99
1.5 6.49 0.99
2.0 8.19 0.97
Number of bead tethering events (ln)
Pause time (s)
C
rVWF-A1 (R1326H)
shear stress (dyn/cm2) koff (s-1) R2
1.0 15.01 0.99
1.25 18.89 0.98
1.5 24.53 0.98
Number of bead tethering events (ln)
Pause time (s)
D
rVWF-A1 (I1309V)
shear stress (dyn/cm2) koff (s-1) R2
0.5 0.56 0.98
0.85 0.73 0.99
1.5 1.19 0.99
3.0 1.54 0.98
Number of bead tethering events (ln)
Pause time (s)
E
rVWF-A1 (I1309V, R1326H)
shear stress (dyn/cm2) koff (s-1) R2
0.5 5.29 0.99
1.0 8.18 0.99
1.5 9.51 0.98
2.0 11.23 0.97
Number of bead tethering events (ln)
Pause time (s)
F
rVWF-A1 (R1326H)
rVWF-A1 (I1309V, R1326H)
rVWF-A1 (WT)
rVWF-A1 (I1309V)
koff (s-1)
Force acting on bond (pN)

Figure 3

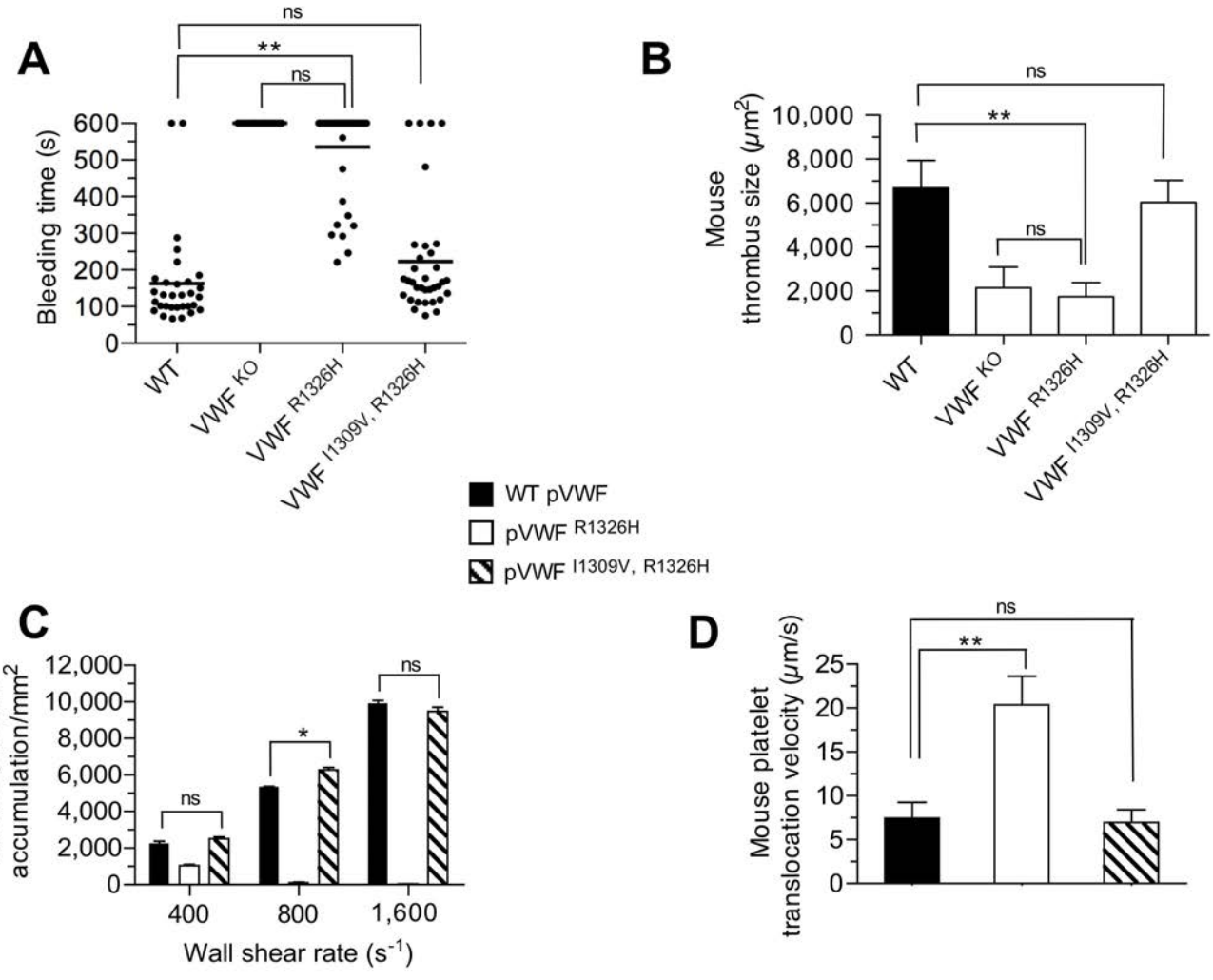
A
Bleeding time (s)
600
500
400
300
200
100
0
ns
**
ns
WT
VWF KO
VWF R1326H
VWF I1309V, R1326H
B
Mouse thrombus size (μm²)
10,000
8,000
6,000
4,000
2,000
0
ns
**
ns
WT
VWF KO
VWF R1326H
VWF I1309V, R1326H
WT pVWF
pVWF R1326H
pVWF I1309V, R1326H
C
Mouse platelet accumulation/mm²
12,000
10,000
8,000
6,000
4,000
2,000
0
ns
*
ns
400
800
1,600
Wall shear rate (s⁻¹)
D
Mouse platelet translocation velocity (μm/s)
25
20
15
10
5
0
ns
**

Figure 4

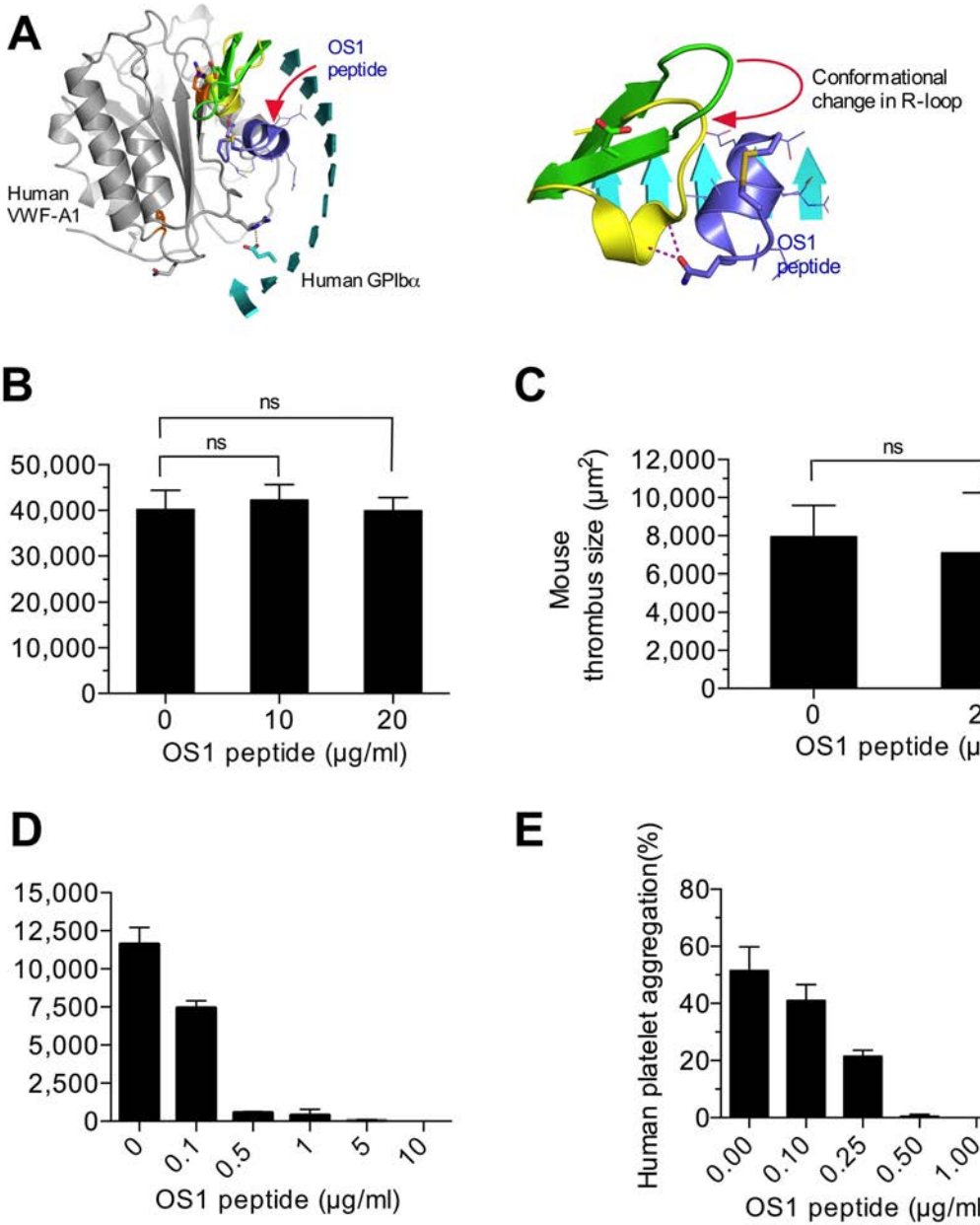
A
OS1
peptide
Human
VWF-A1
Human GPIbα
Conformational
change in R-loop
OS1
peptide
B
ns
ns
Mouse platelet
accumulation/mm2
50,000
40,000
30,000
20,000
10,000
0
0
10
20
OS1 peptide (μg/ml)
C
ns
Mouse
thrombus size (μm2)
12,000
10,000
8,000
6,000
4,000
2,000
0
0
20
OS1 peptide (μg)
D
Human platelet
acummulation/mm2
15,000
12,500
10,000
7,500
5,000
2,500
0
0
0.1
0.5
1
5
10
OS1 peptide (μg/ml)
E
Human platelet aggregation(%)
80
60
40
20
0
0.00
0.10
0.25
0.50
1.00
5.00
OS1 peptide (μg/ml)

Figure 5

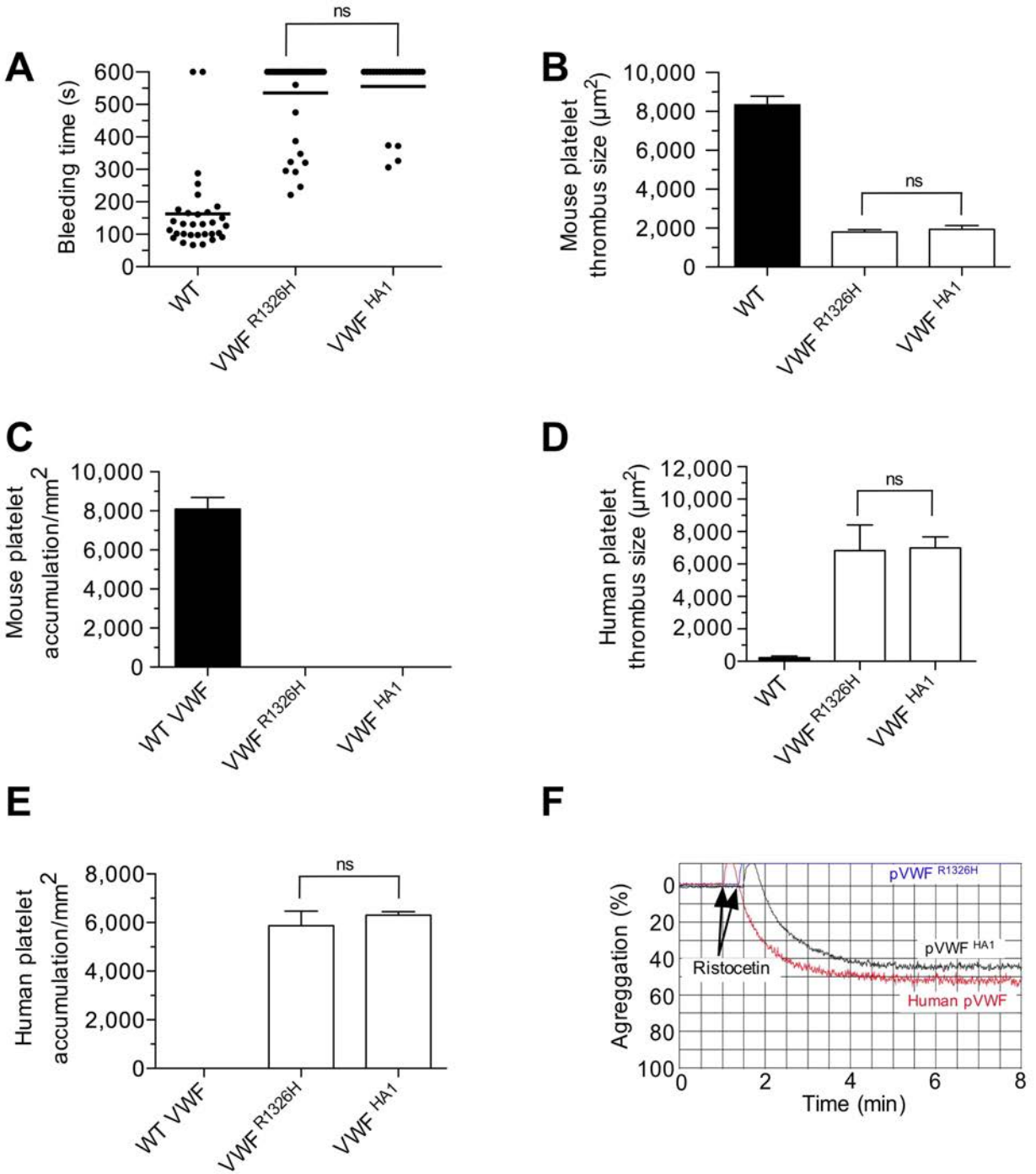
A
Bleeding time (s)
600
500
400
300
200
100
0
ns
WT
VWF R1326H
VWF HA1
B
Mouse platelet thrombus size (µm²)
10,000
8,000
6,000
4,000
2,000
0
ns
WT
VWF R1326H
VWF HA1
C
Mouse platelet accumulation/mm²
10,000
8,000
6,000
4,000
2,000
0
WT VWF
VWF R1326H
VWF HA1
D
Human platelet thrombus size (µm²)
12,000
10,000
8,000
6,000
4,000
2,000
0
ns
WT
VWF R1326H
VWF HA1
E
Human platelet accumulation/mm²
8,000
6,000
4,000
2,000
0
ns
WT VWF
VWF R1326H
VWF HA1
F
Agreggation (%)
0
20
40
60
80
100
pVWF R1326H
pVWF HA1
Ristocetin
Human pVWF
0
2
4
6
8
Time (min)

Figure 6

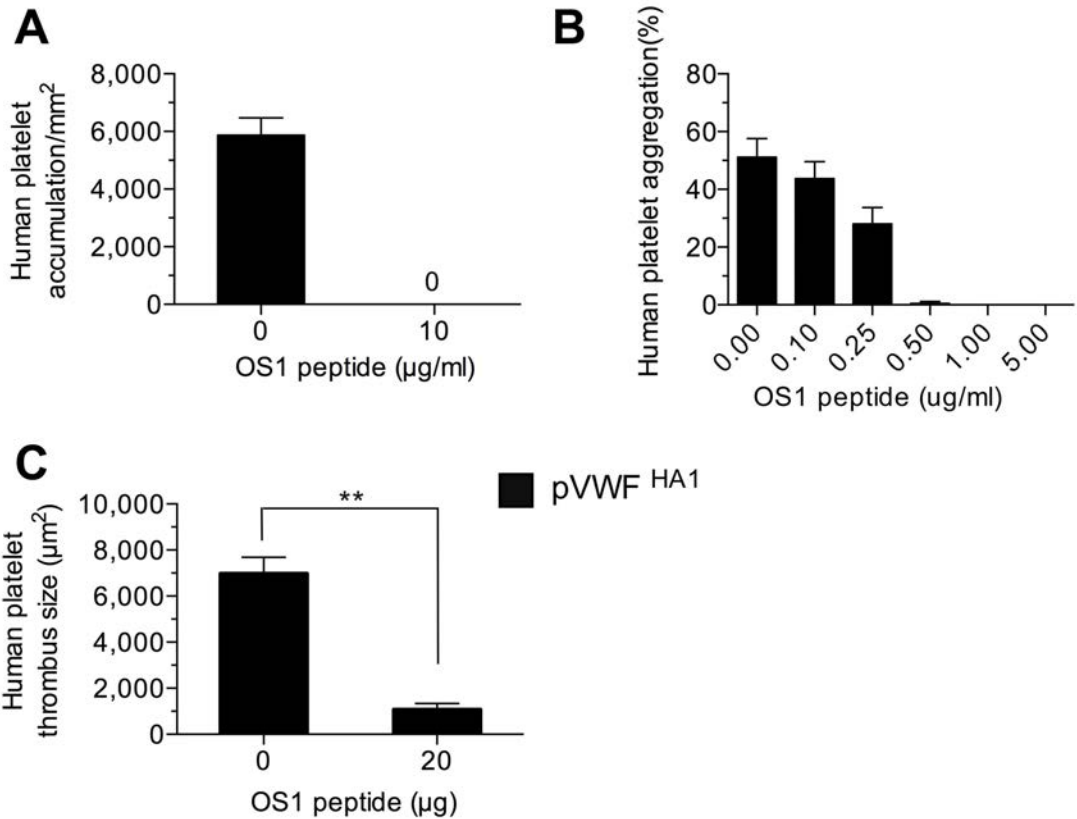
A
Human platelet accumulation/mm2
8,000
6,000
4,000
2,000
0
0
0
10
OS1 peptide (μg/ml)
B
Human platelet aggregation(%)
80
60
40
20
0
0.00
0.10
0.25
0.50
1.00
5.00
OS1 peptide (ug/ml)
C
Human platelet thrombus size (μm2)
10,000
8,000
6,000
4,000
2,000
0
**
0
20
OS1 peptide (μg)
pVWF HA1

Table 1. Intrinsic dissociation rates constants (k^0_{off}) and reactive compliance (σ) values for murine GPIbα–VWF-A1 tether bond

Mouse rVWF–A1	k^0_{off} (s^{-1})	σ (nm)	R^2
WT	3.05 ± 0.55	0.028 ± 0.001	0.97
R1326H	7.80 ± 1.15	0.039 ± 0.002	0.93
I1309V	0.49± 0.04	0.020 ± 0.003	0.95
I1309V, R1326H	4.15 ± 0.67	0.028 ± 0.001	0.94

Values were determined by using maximal likelihood statistical estimates of Bell parameters.